IEEE Access
Multidisciplinary | Rapid Review | Open Access Journal

Received March 7, 2017, accepted March 31, 2017, date of publication April 25, 2017, date of current version June 7, 2017.

Digital Object Identifier 10.1109/ACCESS.2017.2697908

A Low-Complexity Synchronizer for OFDM-UWB-Based Vehicular Communications

XIUWEN YIN[1], JIANQI LIU[2], (Member, IEEE), YONGFENG SU[2], XIAOMING XIONG[1], AND GUOHUA XIONG[3]

[1]School of Automation, Guangdong University of Technology, Guangzhou 510006, China
[2]School of Information Engineering, Guangdong Mechanical & Electrical College, Guangzhou 510515, China
[3]Guangdong Construction Polytechnic, Guangzhou 510440, China

Corresponding author: Jianqi Liu (liujianqi@ieee.org)

This work was supported in part by the Guangzhou Science and Technology Plan Projects under Grant 201604020016, in part by the Guangdong Province Science and Technology Plan Projects under Grant 2016B010108004, in part by the Guangdong Province Special Project of Industry-University-Institute Cooperation under Grant 2014 B090904080, and in part by the Guangdong Natural Science Foundation under Grant 2016A030313734 and Grant 2016A030313735.

ABSTRACT The high implementation complexity of multiband orthogonal frequency-division multiplexing (MB-OFDM) ultra-wideband (UWB) technology is the major hurdle for applying it to vehicular communications. This paper presents a comprehensive synchronizer with low complexity and high performance for the MB-OFDM UWB. A low-complex overall architecture is proposed, in which the sub-functions are divided into amplitude-detection-based functions and phase-detection-based functions. All of the amplitude-detection-based functions are implemented based on a simplified cross correlation-based matched filter, and a serial structure-based auto-correlation block is designed exclusively for carrier frequency offset estimation. Several effective methods for the sub-functions are proposed based on the proposed overall architecture. Evaluation results show that the proposed synchronizer has high performance with low complexity.

INDEX TERMS MB-OFDM, synchronization, UWB, vehicular communication, overall architecture, CFO.

I. INTRODUCTION

Internet of Vehicle (IoV) has been widely studied and applied in recent years [1]. Currently, most of the researches on IoV based high-data-rate transmission are proposed based on IEEE 802.11p or 5G [2], [3]. However, UWB technology, which offers wide bandwidth and low power spectral density (PSD), is also a promising technology for high-speed IoV, especially the applications of short-range communication with strict limitation on power consumption. For example, UWB can be used in the inter-vehicle communication and power-limited in-vehicle communications to obtain low-power consumption and avoid interference to other systems. Some discussions on the efficiency of using UWB technology for vehicular communications have been proposed in recent years [4], [5].

Among the available techniques for UWB, multi-band orthogonal frequency-division multiplexing (MB-OFDM) [6], [7] is one of the most promising techniques for high-data-rate applications, due to its good features such as robustness in dispersive channels and high spectrum efficiency [8]. 5G/ IEEE 802.11p based IoV systems usually adopts network-level methods to reduce power consumption [9]. However, MB-OFDM UWB based systems can achieve low power at both network level and physical level because of the strict PSD limitation on the transceiver. At present, one of the major difficulties of applying MB-OFDM UWB technology to vehicular communications is the high cost brought by the high implementation complexity of MB-OFDM UWB technology.

As time-frequency code (TFC) is adopted in the MB-OFDM UWB system, synchronization in MB-OFDM UWB systems is much more complex than normal OFDM systems. In MB-OFDM UWB systems, synchronization is one of the most complex blocks at the receiver. In addition, MB-OFDM UWB systems are very sensitive to synchronization errors. Timing errors and carrier frequency offsets (CFO) destroy the orthogonality of the OFDM subcarriers, which usually result in severe performance degradation [10]. A low-complex synchronizer with high performance is still one of the major difficulties for the practical system design. Typical digital baseband architecture for the MB-OFDM UWB receiver is shown in Figure 1.

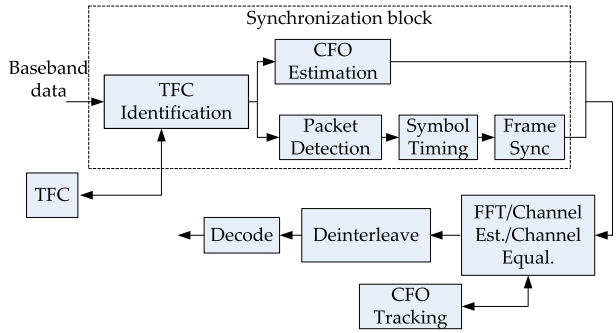

FIGURE 1. A typical digital baseband architecture for the MB-OFDM UWB receiver.

Issues of OFDM-based synchronization have been researched for years, and many effective methods have been proposed [11]–[24], of which some are specific to MB-OFDM UWB systems [12], [15]–[17], [20]–[24]. However, most of these methods focus on designing one or two sub-functions without giving a comprehensive synchronization solution. For example, a low-complex packet detector has been proposed in [12]. A timing offset estimation method has been proposed in [16] based on searching for the first important multipath, which has been shown to have high performance under high SNRs. In [22], a CFO-estimation algorithm with high performance has been proposed based on BLUE principle.

Since auto-correlation (AC) algorithm can be implemented iteratively, most existing comprehensive synchronization solutions with low complexity for OFDM systems are designed completely based on AC operation [21], [26], [27], in which all sub-functions are implemented based on AC. Among these solutions, the scheme in [21], which has very low complexity, is specially designed for MB-OFDM UWB systems. However, this scheme is still not an optimal solution, as AC is much sensitive to noise and that MB-OFDM UWB systems are usually applied to low SNR environments due to the strict PSD limitation on MB-OFDM UWB devices.

Compared to the conventional vehicular ad-hoc network (VANET) physical layer, which is usually applied to the low-data-rate applications such as positioning [28], [29], MB-OFDM UWB technology has much higher implementation complexity. In this paper, we propose a comprehensive synchronizer for MB-OFDM UWB systems, which aims to obtain both high performance and low complexity. A low-complex overall architecture is proposed, which divides the sub-functions into amplitude-detection-based functions and angle-detection-based functions. All of the amplitude-detection-based functions are implemented based on a simplified CC based matched filter (MF), which has low complexity and high noise immunity, and a serial structure based AC block is designed exclusively for carrier frequency offset(CFO) estimation. Based on the overall architecture, several novel methods for the sub-functions are also proposed in this paper.

The main contributions of this article are as follows:

- Differences between AC and CC are systemically compared with a new perspective. By analyzing the role of AC and CC in OFDM synchronization, we found that the functions provided by these two basic operations in OFDM synchronization can be divided into two types: detecting the phase offset between received symbols and obtaining the correlation between symbols through detecting amplitude. Based on this division, we can analyze the differences between AC and CC in the scenarios of ''phase detection'' and ''amplitude detection'', respectively. In this way, the analysis process is much simple and possible and the results are reliable.
- A low-complex overall architecture with dual common blocks is proposed. In contrast with the conventional AC-based low-complex synchronization solutions of OFDM systems, we proposed a high performance and very low-complex overall architecture, which includes both AC and CC operation, for MB-OFDM systems.
- We proposed an effective comprehensive synchronization solution for MB-OFDM based UWB systems. A CC-based low-complex TFC identification method is proposed based on a defined seven-point time sequence, and a joint packet detection and timing offset estimation structure based on multiple thresholds and energy accumulation is designed. We also proposed an effective CFO estimation method, in which a serial AC structure is designed to achieve low complexity.

The rest of this paper is organized as follows. Materials and methods are shown in section II. Evaluation results and discussion are presented in Section III. Section IV concludes the paper.

II. MATERIALS AND METHODS

A. SYSTEM MODEL

The Federal Communications Commission (FCC) has allocated 7500MHz spectrums from 3.1-10.6GHz for UWB applications, and UWB devices are required to occupy at least 500MHz with a PSD less than -41.25dBm/MHz [30]. MB-OFDM UWB technology divides the entire 7500 MHz spectrums into fourteen 528 MHz bands [31]. In MB-OFDM UWB systems, a symbol includes $N = 128$ IFFT samples, $N_z = 32$ null prefix samples and $N_g = 5$ null guard samples. Of these 128 sub-carriers, 122 sub-carriers are used, including 100 data sub-carriers, 12 pilot sub-carriers and 10 guard sub-carriers. The important parameters of MB-OFDM UWB technology are shown in Table 1.

In MB-OFDM UWB systems, preamble symbols are adopted for synchronization. The standard preamble sequence defined in [6] consists of 21 packet synchronization (PS) symbols, 3 frame synchronization (FS) symbols and 6 channel estimation (CE) symbols. Of them, the PS symbols are used for timing and frequency synchronization, and the FS symbols are designed for frame synchronization.

A modified S-V channel model is adopted for the UWB channel [32]. The channel impulse response (CIR) can be

TABLE 1. Important parameters of MB-OFDM UWB.

Parameter	Value
FFT size	128
number of data subcarriers	100
number of pilot subcarriers	12
Bandwidth	528MHz
subcarrier frequency spacing	4.125MHz
FFT period	242.42ns
power spectral density	<-41.25dBm/MHz

given by

$$h_t = X \sum_{l=0}^{L} \sum_{k=0}^{K} a_{k,l}\delta(t - T_l - \tau_{k,l}) \tag{1}$$

where X is the log-normal shading, T_l is the delay of the lth cluster, $\tau_{k,l}$ is the kth ray delay related to the lth cluster and $a_{k,l}$ is the multipath gain coefficient.

Let $s(n)$ be the transmitted sample sequence, the received signal $r(n)$ is given by

$$r(n) = \sum_{i=0}^{l-1} s(n - i - \theta)h_i e^{j2\pi\varepsilon\frac{n}{N}} + v(n) \tag{2}$$

where l is the length of channel impulse response, n is the time index of the received sample, θ and ε represent the timing offset and CFO, respectively, and $v(n)$ is Gaussian noise with zero mean and variance σ^2.

B. COMPARISON OF BASIC OPERATIONS

Currently, AC and CC are still the two most widely used effective basic operations for the OFDM based synchronization. However, it is still controversial about whether AC or CC is more suitable. It had better first identify the advantages and disadvantages of the basic operations in terms of performance and implementation complexity before the designing of the synchronizer, as it is of great value to guide the overall architecture design.

It is easy to get the conclude that the AC has much lower complexity than CC, as AC can be implemented with low-complex iterative structure, which is also the main reason of why most of the low-complex OFDM synchronization solutions are designed based on AC. However, the comparison on performance between AC and CC is much more complicated. By analyzing the role of the AC and CC in OFDM synchronization, we found that the functions provided by the basic operations in OFDM synchronization can be divided into two types: detecting the phase offset between received symbols and obtaining the correlation between symbols through detecting amplitude. In terms of the ''phase detection'' function, AC is a much better choice than CC, as the phase offset between received symbols can not be obtain through CC operation. However, for the ''amplitude detection'' function, both AC and CC are widely used. As the ''amplitude detection'' performance of AC and CC are mainly depend on the anti-noise performance of them, the comparison on ''amplitude detection'' can be done through analyzing the anti-noise performance of AC and CC.

Assuming that $r(n + k)(k = 0, \ldots, N - 1)$ and $r(n + W + k)(k = 0, \ldots, N - 1)$ are the samples of two received preamble symbols, the amplitude of the AC output can be given by.

$$\begin{aligned} AC_n &= \sum_{k=1}^{N} r(n+k)^* r(n+k+W) \\ &= \sum_{k=1}^{N} (|\sum_{i} s(n+k+i)h_i|^2 + v_{ac}) \end{aligned} \tag{3}$$

where

$$\begin{aligned} v_{ac} &= v(n+W+k)\sum_{i} h_i^* s(n+k+i)^* + v(n+k)^* \\ &\quad \times \sum_{i} h_i s(n+k+i) + v(n+k)^* v(n+W+k) \end{aligned} \tag{4}$$

The output of CC is given by.

$$\begin{aligned} CC_n &= \sum_{k=1}^{N} r(n+k)^* s(n+k) \\ &= \sum_{k=1}^{N} [s(n+k)\sum_{i} s(n+k)^* h_i^* + v_{cc}] \end{aligned} \tag{5}$$

where

$$v_{cc} = s(n+k)v(n+k)^* \tag{6}$$

From (4) and (6), it can be seen that noise has a greater impact on AC_n than CC_n.

The simulated ''amplitude detection'' performance of AC and CC under the SNR environments of -6db and -3db are shown in Figure 2. In the simulation, the used PS symbols are set following the PS symbol definition of TFC 1 in specification [6]. In the figure, the amplitude distributions of the AC and CC in the scenarios of PS symbols are received and that noise is received are simulated, respectively. The figure shows that the received PS symbols can be distinguished from noise with a high probability based on the outputs of CC, while the AC outputs of the two scenarios are highly overlapped, which means that CC can obtain much better amplitude-detection performance than AC under low SNR environments.

C. SYNCHRONIZER DESIGN

1) OVERALL ARCHITECTURE

In term of function implementation, we found that the individual synchronization functions in OFDM UWB systems can be divided into two types: the ''amplitude-detection'' type and the ''phase-detection'' type. The timing-related individual functions, such as packet detection and symbol timing, have a same basic operation, detecting the amplitude of the AC/CC output, though the operation details of them are

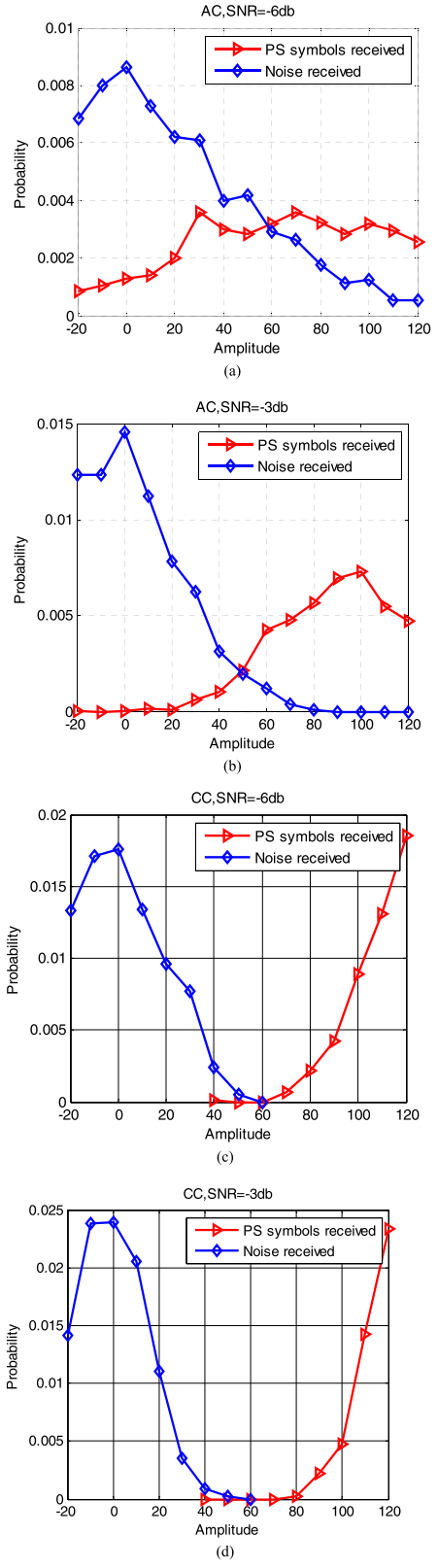

FIGURE 2. Amplitude detection comparison between AC and CC. (a) AC, SNR=−6db; (b) AC, SNR=−3db; (c) CC, SNR=−6db; (d) CC, SNR=−3db.

different. However, the CFO estimation needs a completely different basic operation, which can generalized as detecting the phase of the output.

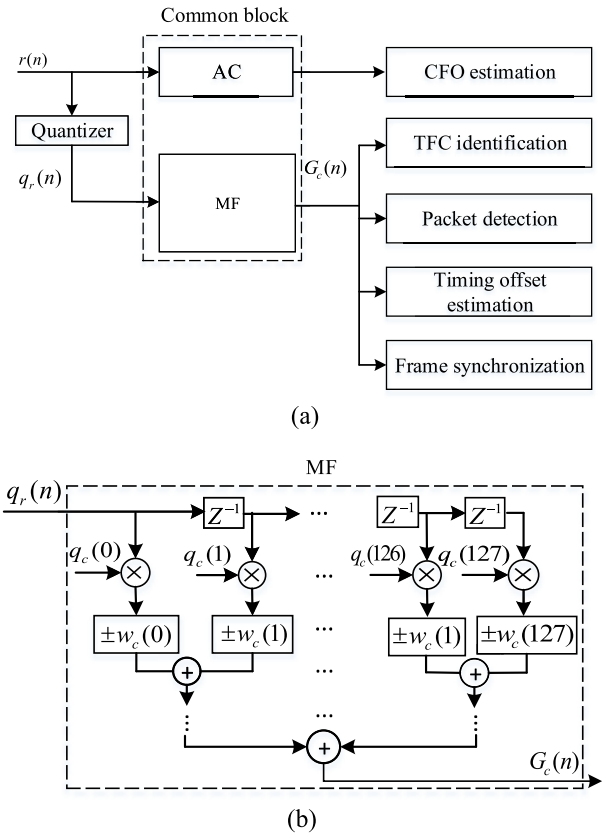

FIGURE 3. Structure of the overall architecture. (a) The Overall architecture; (b) the MF.

In MB-OFDM UWB systems, the fine timing synchronization should be implemented in the synchronization block before FFT, but the fine frequency synchronization is usually not included in the synchronization block, which is usually implemented after FFT alone. Therefore, an effective synchronization solution for the MB-OFDM UWB system should first ensure the performance of the timing synchronization and then pursue low complexity. Based on the preceding analysis in section II, we know that AC is more sensitive to noise than CC in the case of amplitude detection. Therefore, in contrast with conventional OFDM-based low-complex synchronization solutions, which are designed only based on AC, the proposed overall architecture is designed based on two common blocks: an AC block and a matched filter (MF), as shown in Figure 3. The AC block is implemented iteratively based on a serial structure and the MF can be considered as a simplified CC block. All the ''amplitude-detection'' based functions, are implemented based on the MF output, and only the CFO estimation, which is of ''phase-detection'' type, is implemented based on AC. Based on this ideal, sub-functions of TFC identification, packet detection, timing offset estimation and frame synchronization are implemented based on the MF output in the proposed architecture.

The MF is designed based on the low-complex PSMF structure in [33]. To maintaining a relatively high performance, the PSFM structure simplifies the CC operation by

rounding the decimal preamble symbol coefficients into integer, which means the total complexity of the adders in the PSMF is still much high. As there are big differences on implementation details between the "amplitude-detection" functions, it is better to improve the performance of the functions through optimizing the implementation process of the individual functions rather than through optimizing the performance of the common block. According to specification [7], the preamble symbol coefficients of a designed UWB system is fixed. Therefore, we can map the fixed coefficients to the simpler weighting coefficients to future reduce the complexity of the PSMF with little performance decrease.

The designed tree structure based MF block is shown in Figure 3(b), in which $q_r(n)$ is the sign bit of $r(n)$, $q_c(k)(k = 0, .., 127)$ are the sign bits of coefficients $c(k)(k = 0, \ldots, 127)$ (belonging to preamble type c) and $w_c(k)$ is the weighting coefficient for $c(k)$. Most $w_c(k)$ can be given by

$$w_c(k) = \begin{cases} 0 & |c(k)| \le 0.5 \\ 1 & 0.5 < |c(k)| \le 1.5 \\ 2 & 1.5 < |c(k)| \end{cases} \quad (7)$$

As both $q_r(n)$ and $q_c(k)$ are sign bits, each multiplication $q_r(n)q_c(k)$ in the MF can be implemented with a NXOR gate. Then, if $q_r(n)q_c(k) = 1$, $w_c(k)$ is outputted as the input to the first layer of the adder-tree structure, else $-w_c(k)$ is outputted. As the coefficients used in the MF is fixed, some mapping rule different from the rule in formula (7) can and should be adopted for few special coefficients to ensure the adder-tree structure has very low complexity. Taking the first-layer adders in the adder tree as examples, a special mapping rule should be applied to avoid the binary addition result longer than 3bit, which means that if $|w_c(0)| > 1.5$ and $|w_c(1)| > 1.5|$, the coefficient with smaller absolute value should be mapped as 1 to ensure $| \pm w_c(0) \pm w_c(1)| < 4$. Based on these methods, the MF can be implemented with approximately 128 NXOR gates and 48 2-bit 48 3-bit adders, 24 4-bit adders, 8 5-bit adders and 4 6-bit adders, and the major hardware cost of the AC block is one complex multiplier and two complex adders. Therefore, the proposed overall architecture has very low complexity and the whole synchronizer will have very low complexity if all the individual functions can be implemented by adopting only the basic operations provided by the common blocks in the overall architecture.

2) TFC IDENTIFICATION

TFC is adopted in MB-OFDM UWB systems to spread data transmission over multiple sub-bands. Multiple TFC types corresponding with multiple preamble patterns are adopted in MB-OFDM UWB technology to give convenience for multi-user access. The existing low-complex TFC identification methods are commonly implemented based on AC, such as the method in [21]. However, as aforementioned, AC-based TFC identification methods are not suitable for "amplitude detection" in low SNR environments.

In specification [6], ten TFC types corresponding to ten preamble patterns are defined. This means that if the TFC identification is implemented directly based on CC, ten CCs need to be executed simultaneously when a new symbol is received, which would leads to a very complex structure. However, if the signal is detected on the sub-bands according to the seven-points time sequence shown in Figure 4, in which each point has a time span equal to the length of a symbol, much fewer CCs are needed to detecting the received symbol. For example, only TFC 3 and TFC 4 need to be identified at the sixth point.

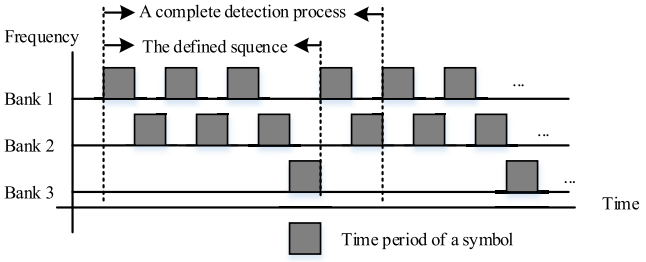

FIGURE 4. The designed hoping sequence.

Based on the time sequence shown in Figure 4, Table 2 gives the preamble patterns that are used to match the received signal at each sequence point. Based on this assignment, all of the TFC types defined in specification [6] can be identified within a nine-point time sequence. For example, if TFC 1 is used in the MB-OFDM UWB system, the TFC type will be identified at either the first, the third or the fifth sequence point if there are PS symbols present. Using the TFC identification process in Table 2, at most three TFC types are needed to identify the TFC type of the received symbol, which means that the TFC identification block can be implemented by using three MFs.

TABLE 2. The TFC types assigned for each sequence point.

Sequence point	The identified TFC types
1	TFC 1, 2, 8
2	TFC 3, 4, 10
3	TFC 1, 2, 5
4	TFC 3, 4, 6
5	TFC 1, 2, 9
6	TFC 3, 4,
7	TFC 7, 9, 10

It will still greatly increase the complexity of the synchronization overall architecture if the TFC identification block is directly implemented by using three MFs based on the TFC identification process in Table 2, as two additional MFs need to be added to the overall architecture. To avoid increasing the complexity of the overall architecture, a parallel-serial conversion based TFC identification structure is proposed, as shown in Figure 5, in which only one MF block is used. The three preamble patterns used for matching the received

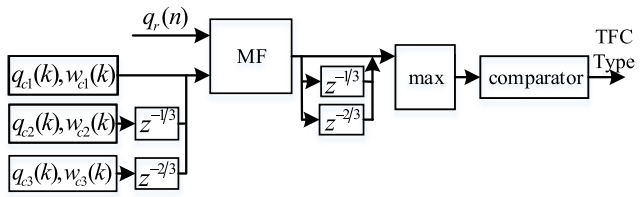

FIGURE 5. Structure of the proposed TFC identification scheme.

symbol are serially loaded into the MF with a time delay of 1/3 of the sampling period.

The shortcoming of the structure is that the allowed maximum operation delay of the MF should be shortened to 1/3 of the sampling period. However, as the multilayer adder tree structure can introduce pipeline to the matching-operation process, the MF can completed the operation within the time interval of 1/3 of the sampling period without increasing implement complexity.

3) PACKET DETECTION

In MB-OFDM UWB systems, the error results of the TFC identification block can be easily corrected by the following packet detection block. However, the error caused by packet detection cannot be corrected by the following synchronization functions, which means that packet detection in MB-OFDM UWB systems should have much higher performance than TFC identification. Another major issue of packet detection design is that the performance of packet detection is highly dependent on the threshold. The most widely used method to alleviate the issue is adopting relative thresholds, for example, the method in [26]. However, those methods usually cause a great increase in implementation complexity because the signal power need to be additionally estimated in them.

Based on the MF block, we propose a multi-threshold-based packet detector, in which multiple detections are adopted, as shown in Figure 6. In the figure, M is the number of the required detection times of a complete packet detection process and $\lambda_i (i = 1, \ldots, M)$ are the thresholds corresponding to the detections. The packet detection structure is implemented in an iterative manner, in which

$$D_i = D_{i-1} + G(n) \tag{8}$$

where $D_{i-1} = D_{i-2} + G(n - N_s)$ and the initial value $D_0 = 0$. If $D_M > \lambda_M$, a packet is detected.

Packet detection errors include false alarms and missed detections. The threshold with large value is required to get low false alarm probability, but a small threshold is required for low missed detection probability. In conventional packet detection methods, thresholds with precise values are usually needed to meet the performance requirements from both false alarms and missed detections. In the proposed packet detection structure, the multiple detections based process can be used to alleviate threshold dependence, through which low false alarm probability can be achieved. Without consideration of the false alarm probability, $\lambda_i (i = 1, \ldots, M)$ can be set with relatively small values to pursue low missed detection probability, which means precise values are no longer needed for the thresholds. To avoid high missed detection probability, the threshold λ_1 should be set to a very small value. As D_i with larger i is more robust, the threshold value for λ_i can increase gradually with increasing i according to inequality $\lambda_i > \lambda_{i-1} + \lambda_1$. In this way, a fixed value for $\lambda_i (i = 1, \ldots, M)$ is suitable for a much large range of SNR environments.

4) TIMING OFFSET ESTIMATION

After packet detection, the timing offset, which is the offset between the real FFT starting boundary (n^*) and the time index ($\tilde{n}$) at which the packet is detected, should be estimated. In MB-OFDM UWB systems, timing offset estimation easily "lock" onto the strongest path due to the first significant multi-path is usually not the strongest in UWB channels [34]. Several methods [16], [35] have been proposed to find the first significant multi-path by exploiting the polarity of the FS symbol, which is opposite to the PS symbol. However, these methods are not suitable for low SNR environments due to the high noise sensitivity.

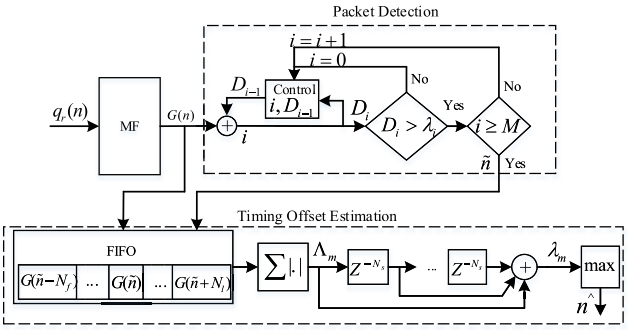

FIGURE 6. Joint structure of packet detection and timing offset estimation.

Based on the MF block, the proposed timing offset estimation structure is shown in Figure 6. As aforementioned, the first significant multi-path in UWB channels is not necessarily the strongest path. However, the maximum value of the accumulated energy can be obtained by accumulating the multi-path energy starting from the first significant path. As shown in Figure 6, the accumulated value is expressed as

$$\Lambda(m) = \sum_{i=m}^{m+N_c} |G(m)| (\tilde{n} - N_l \leq m \leq \tilde{n} + N_l) \tag{9}$$

where $\tilde{n}$ is the time index where the packet is detected, N_c is the length of the window which is used to accumulate the multi-path energy and N_l is the highest radius used to search the real starting boundary around $\hat{n}$. In practical applications, the multi-path length of the channel is usually unknown. However, the multi-path power in the UWB channel follows a double-exponential decay with the time delay [29], in which the power of front-part paths decays quickly with the time delay. Therefore, N_c can be simply set

to a fixed value, such as $N_g/2$. Also, N_l can be set to a fixed value, since the distance between $\tilde{n}$ and n^* is shorter than N_g.

Although the timing offset can be estimated without adopting threshold based on the accumulated multi-path power, the estimation result is also sensitive to noise. However, in contrast with the methods in [16] and [30], repeated PS symbols can be exploited to further improve performance based on the accumulated multi-path power. By using the repeated PS symbols, Λ_m of P adjacent symbols can be accumulated, as shown,

$$\Gamma(m) = \Lambda(m) + \Lambda(m + N_s) + \ldots + \Lambda(m + PN_s) \quad (10)$$

The starting boundary point n^* can then be estimated as

$$\hat{n} = \arg\max\{\Gamma(\tilde{n} - N_l) \ldots \Gamma(\tilde{n}) \ldots \Gamma(\tilde{n} + N_l)\} \quad (11)$$

5) CARRIER FREQUENCY OFFSET ESTIMATION

MB-OFDM UWB systems are usually applied in high data rate environments. For example, the highest data rate supported in specification [6] is as high as 1Gb/s. It means that a structure with multiple parallel multipliers or complicated multiplier should be adopted in the traditional AC block to meet the strict time delay requirement, in which the maximum delay of the complex multiplication is the sampling interval.

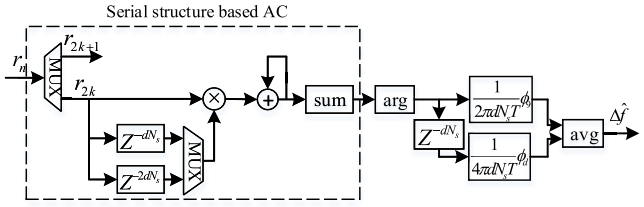

FIGURE 7. The proposed CFO estimator based on a $N/2$-point AC with two-level serial structure.

In contrast with the conventional low-complex OFDM-based synchronizers, the AC block in our proposed synchronizer is designed exclusively for CFO estimation, which means that the AC block can be further optimized to reduce complexity. Based on the proposed overall architecture, the designed CFO estimator is shown in Figure 7. In the estimator, only partial samples of a symbol are used in the AC block to participate in the correlation operation. In Figure 7, the AC block only uses half of the samples (the even samples), which means that the time delay limitation for the complex multiplication is extended to two sampling intervals. Similarly, if the half-samples-based structure still can not meet the time delay requirement, the AC block can be further simplified by using a quarter of the samples based on the overall architecture, which means the time limitation for the complex multiplication can be further extended to four sampling intervals.

Shortening the window length of AC to $N/2$ or $N/4$ will introduce higher noise sensitivity to the AC operation and ultimately degrade the CFO estimation performance. However, the repeated PS symbols can be used to solve this problem. In Figure 7, a two-level serial structure based $N/2$-point AC is designed to avoid performance degradation, in which three PS symbols are adopted to convert one N-point AC operation to two serial $N/2$-point AC operations. In the figure, the estimated CFO is given by

$$\Delta\hat{f} = \frac{1}{2}\left[\frac{1}{2\pi dN_sT}\arg\left(\sum_{k=1}^{N/2} r(n+2k)^* r(n+2k+dN_s)\right) + \frac{1}{4\pi dN_sT}\arg\left(\sum_{k=1}^{N/2} r(n+2k)^* r(n+2k+2dN_s)\right)\right] \quad (12)$$

where arg(.) is used to get the argument of a complex number and avg(.) is the function of getting average.

III. RESULTS AND DISCUSSION

In this section, we evaluate the proposed synchronizer. The complexity of the proposed synchronizer is firstly evaluated. Then, we analyze and simulate the performance of the individual functions. The parameters used in the simulations follow the specifications in [6]: $N = 128$, $N_s = 165$, the carrier frequencies are {3432, 3960, 4488}MHz, and the sub-carrier spacing is 4.125MHz.

A. COMPLEXITY OF THE OVERALL ARCHITECTURE

The synchronizer in MB-OFDM UWB systems is a multi-task block. The individual functions of different synchronizers have different performances. Therefore, it is difficult and meaningless to compare on the whole complexities between synchronizers. However, as all of the individual functions in most existing MB-OFDM UWB based synchronizers are implemented based on basic operations such as AC and CC, these basic operations contribute the major hardware costs of the synchronizer. Therefore, we only need to evaluate the complexity of the overall architecture rather than the complexity of the whole synchronizer.

Based on AC, a comprehensive synchronizer with low complexity is proposed for MB-OFDM UWB systems in [21], which can be used to compare the complexity with the proposed synchronizer. The major hardware costs of the overall architecture in [21] are a four-parallel-AC structure, which is the common block of the overall architecture. However, the four-parallel-AC structure can only identify the seven TFC types defined in specification [36]. To identify the ten TFC types defined in specification [6], the parallel-AC structure in [21] requires at least six AC blocks. Therefore, the major hardware costs of the overall architecture in [21] are six AC blocks. Also, the major hardware costs of our proposed synchronizer are the common blocks. There are two common blocks in our proposed synchronizer, a MF and an AC.

The comparison on the complexity between the proposed overall architecture and the overall architecture in [21] is shown in Table 3. In the proposed overall architecture,

TABLE 3. The comparison on implementation complexity between the proposed overall architecture and the architecture in [21].

Hardware resource	Proposed	Scheme in [21]
complex multiplier	1	6
real adder	11	24
real comparator	17/3	6
complex ABS	0	6

the major components of the AC block are one complex multiplier and two complex adders, and the adders in the MF can be implemented with approximately 96 3-bit adders, 24 4-bit adders and 4 5-bit adders, of which the complexity is approximately equal to eight 32bit real adders. Thus, the major hardware costs of the MF are roughly 128 XNOR and eight real adders. Based on that one complex multiplier can be implemented with three real multipliers and five real adders, one complex adder can be implemented with two real adders, and the complexity of 32 XNOR gates is lower than one real adder, we obtain the results in Table 3. From the table, it is obvious to see that the proposed overall architecture has a much lower complexity than the design in [21]. Additionally, in high data rate applications, the AC blocks in [21] will need to be implemented by using parallel-structure or complicated multiplier, which will exponentially increase the implementation complexity.

B. PERFORMANCE OF TFC IDENTIFICATION

When a new symbol is received, the identification errors of the proposed TFC identification method can be divided into two types:

a) Wrong identification. When a PS symbol with preamble type i is received, if TFC i is not identified or TFC $j(j \neq i)$ is identified under the situation that preamble type i has been loaded in the MF, wrong identification occurs. Therefore, the probability of wrong identification can be given by

$$P_{t\_m} = P[G_i(n) < \lambda_t] + 2P[G_i(n) > \lambda_t]P[G_j(n) > G_i(n)] \quad (13)$$

where i is the TFC type used in the MB-OFDM UWB system, j belongs to the two other TFC types loaded in the MF and λ_t is the threshold. According to (25) in appendix A, P_{t_m} can be given by

$$P_{t\_m} \approx [1 - P_1(\lambda_t)] + 2\sum_{i=\lambda_t}^{N} [P_1(i) - P_1(i-1)]\, P_2(i) \quad (14)$$

b) False alarm. When noise is received, false alarm occurs if a TFC type is identified. According to (26) in appendix A, the probability of false alarm can be given by

$$P_{t\_f} = 3P[G_c(n) > \lambda_t] = 3P_2(\lambda_t) \quad (15)$$

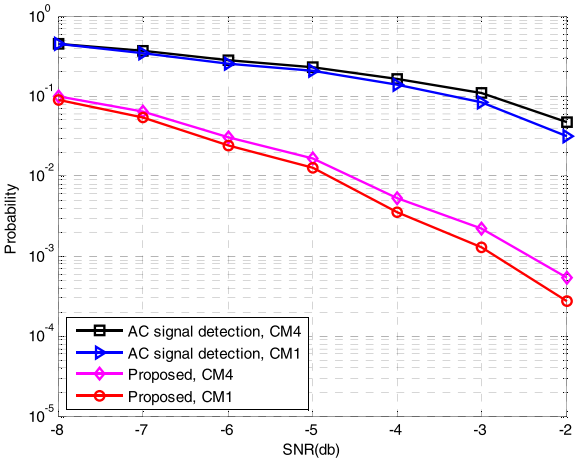

FIGURE 8. Error probabilities of identifying a newly received symbol in UWB channels CM1 and CM4, under adopting the proposed TFC identification method and the signal detection based on single AC, respectively.

By setting an appropriate value for λ_t, the error probability of identifying a newly received symbol can be approximately given by

$$P_{t\_e} = P_{t\_m} + P_{t\_f} \approx [1 - P_1(\lambda_t)] + 3P_2(\lambda_t) \quad (16)$$

According to (25) and (26) in appendix A, P_{t_e} can be given by

$$P_{t\_e} \approx \Phi\left[\frac{\frac{N+2\lambda_t}{4} - \frac{1}{2}erfc\left(\frac{-\tilde{m}}{\sqrt{2\sigma^2}}\right)N}{\sqrt{\frac{1}{2}erfc\left(\frac{-\tilde{m}}{\sqrt{2\sigma^2}}\right)\left[1 - \frac{1}{2}erfc\left(\frac{-\tilde{m}}{\sqrt{2\sigma^2}}\right)\right]N}}\right] + 3\left[1 - \Phi\left(\frac{\frac{N+\lambda_t}{2} - \frac{1}{2}N}{\frac{1}{2}\sqrt{N}}\right)\right] \quad (17)$$

The error probability of identifying a newly received symbol is also simulated in UWB channels CM1 and CM4, as shown in Figure 8. As a comparison, the error probability of the signal detection based on a single AC is also simulated. The simulation is done by assuming TFC 1 is used in the MB-OFDM UWB system and that all used thresholds are optimized by searching for the optimal values for each SNR environment. It is obvious to see from Figure 8 that the error probability of the proposed TFC identification scheme is much lower than the AC based signal detection, although the single signal detection based on AC can only detect the presence of the PS symbol (multiple signal detections are needed to identify the TFC type, which will increase the error probability).

To identify the TFC type, an identification process needs to be executed in both the proposed TFC identification method and the method in [21]. The simulated error probabilities of the complete TFC identification process of the proposed TFC identification method and the method in [21] are shown in Figure 9 and Figure 10. The results are achieved by dividing the simulation process into two steps. First, the wrong

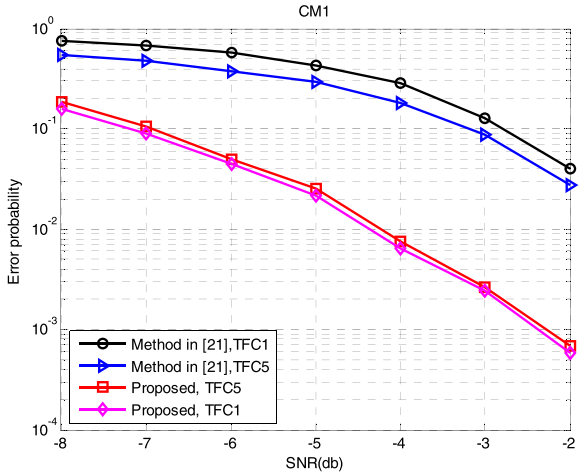

FIGURE 9. Error probabilities of the complete TFC identification process in the UWB CM1 channel, under TFC 1 and TFC 5, respectively.

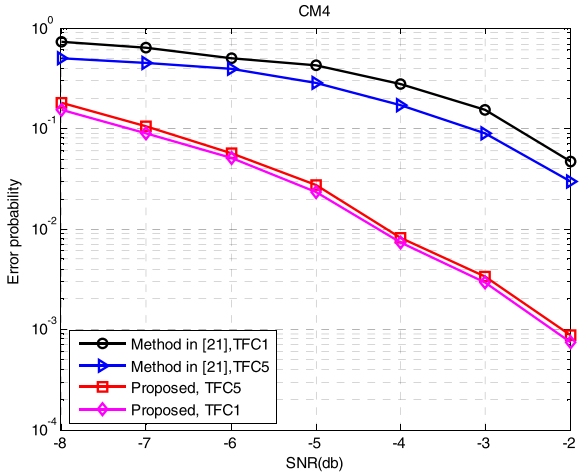

FIGURE 10. Error probabilities of the complete TFC identification process in the UWB CM4 channel, under TFC 1 and TFC 5, respectively.

identification probability is simulated by sending repeated PS symbols. Then, by adopting the same thresholds used to simulate the wrong identification probability, the false alarm probability is simulated under the situation that the received signal is noise. The simulation is done in UWB channels CM1 and CM4 by assuming that TFC 1 and TFC 5 are used in the MB-OFDM UWB system, respectively. As the MF has much better noise immunity than AC, the proposed TFC identification method has much lower error probabilities than the method in [21] in $-8\sim-2$db SNRs.

C. PERFORMANCE OF PACKET DETECTION

The performance of packet detection can also be evaluated through error probability. The error probability of packet detection consists of two parts: the false alarm probability and missed detection probability. The missed detection probability can be defined as the probability that the packet detector does not detect the packet within the time range from the first received PS symbol to the Mth PS symbol. Therefore, the missed detection probability of the proposed packet detector can be given by

$$P_{p\_m} = P[D(1) < \lambda_1] + \sum_{i=2}^{M} \left\{ P[D(i) < \lambda_i] \prod_{j=1}^{i} P[D(j) > \lambda_j] \right\} \tag{18}$$

According to (27) in appendix B, P_{p_m} is given by

$$P_{p\_m} = [1 - P_3(1, \lambda_1)] + \sum_{i=2}^{M} \left\{ [1 - P_3(i, \lambda_i)] \prod_{j=1}^{i} P_3(j, \lambda_j) \right\} \tag{19}$$

The false alarm probability can be defined as the probability that the packet detector "gets" the PS symbol when noise is transmitted. Therefore, according to (28) in appendix B, the false alarm probability of the proposed packet detector is given by

$$\begin{aligned} P_{p\_f} &= \prod_{i=1}^{M} P[D(i) > \lambda_i] \\ &= \prod_{i=1}^{M} P_4(i, \lambda_i) \end{aligned} \tag{20}$$

Therefore, the error probability of the proposed packet detector can be given by

$$\begin{aligned} P_{p\_e} &= P_{p\_m} + P_{p\_f} \\ &\approx \sum_{i=1}^{M} [1 - P_3(i, \lambda_i)] + \prod_{i=1}^{M} P_4(i, \lambda_i) \\ &\approx \sum_{i=1}^{M} \Phi \left[\frac{\frac{iN+2\lambda}{4} - \frac{1}{2} erfc\left(\frac{-\tilde{m}}{\sqrt{2\sigma^2}}\right) iN}{\sqrt{\frac{1}{2} erfc\left(\frac{-\tilde{m}}{\sqrt{2\sigma^2}}\right)\left[1 - \frac{1}{2} erfc\left(\frac{-\tilde{m}}{\sqrt{2\sigma^2}}\right)\right] iN}} \right] \\ &\quad + \prod_{i=1}^{M} \left[1 - \Phi \left(\frac{\frac{iN+\lambda}{2} - \frac{1}{2} iN}{\frac{1}{2}\sqrt{iN}} \right) \right] \end{aligned} \tag{21}$$

The comparison on error probability between packet detectors is shown in Figure 11 and Figure 12. The traditional AC based method [21], and the sign-bit based scheme in [12] are included in the comparison. All of the methods in Figure 11 and Figure 12 require at least two PS symbols to detect a "packet". Therefore, we assume that two PS symbols are used for packet detection and that TFC 1 is used in the MB-OFDM UWB system in the simulation, which means that the parameter M in the proposed packet detector needs to be set as $M = 2$. The simulation is done in UWB channels CM1 and CM4. Two scenarios of the threshold setting, the threshold is set with a fixed value for all of the SNRs ($-8\sim-2$db) and the threshold is set with optimal value for each SNR environment, are simulated, respectively. In the "fixed value" case, the fixed value is selected using the criterion that the average error probability

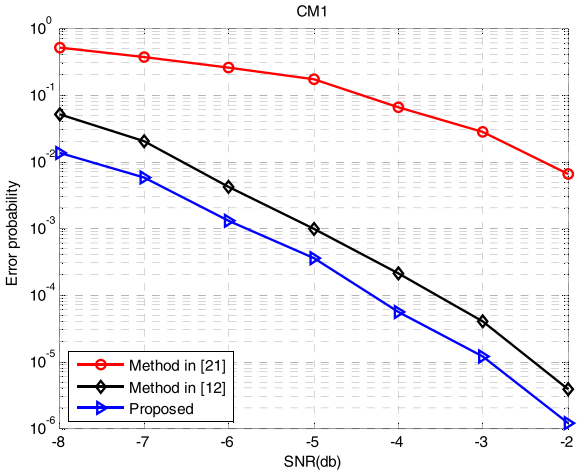

FIGURE 11. Comparison of error probabilities between packet detection methods, in UWB CM1.

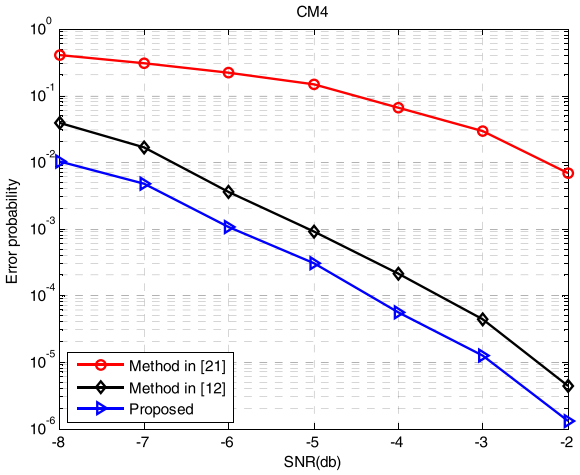

FIGURE 12. Comparison of error probabilities between packet detection methods, in UWB CM4.

under SNR range [−8db,−2db] has minimum value. The proposed packet detector and the scheme in [12] have much better performance than the method in [21] in low SNR environments (−8 ∼ −2db) because the better noise immunity of them. It also can be seen that the error probabilities at ''edge'' SNRs (i.e. -8db and -2db) of the ''fixed value'' case are higher than the ''optimal value'' case and that the performance degradation of the proposed packet detector is much smaller than the method in [12], which means that the performance of the proposed scheme is much less dependent on the threshold then the method in [12]. Also, it can be seen that the proposed packet detector has better performance than the method in [12].

D. PERFORMANCE OF TIMING OFFSET ESTIMATION

The performance of timing offset estimation can be evaluated using minimum square error (MSE), which has a mathematical expression given by

$$MSE = \frac{1}{M}\sum_{M}(\hat{n} - n^*)^2 P(\hat{n}) \tag{22}$$

where $\hat{n}$ is the time index that be estimated as the starting boundary of the symbol, n^* is the real starting point and $P(\hat{n})$ is the probability that n^* is estimated to be at $\hat{n}$.

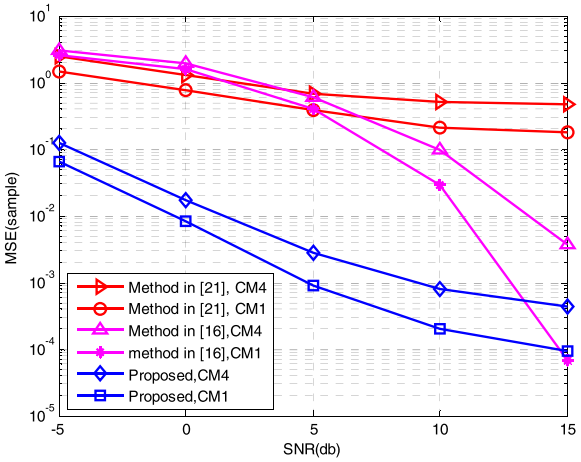

FIGURE 13. Comparison of MSEs between timing offset estimation methods.

The comparison on MSE between timing-offset estimators is shown in Figure 13. Besides the AC-based method in [21], the FTA method in [16] is also included in the comparison, which is a typical method of searching for the first significant multipath of the UWB channel. Of the three schemes, only the method in [16] is implemented based on threshold. By setting $P = 4$ for the proposed timing offset estimator, the simulations are done in UWB channels CM1 and CM4, and the threshold used in the method in [16] is set with the optimal values of each SNR environment. It can be seen from Figure 13 that the method in [21] has much high MSEs across the whole SNR range from -5db to 15db, because it easily ''locks on'' the strongest multipath in UWB channels. Under high SNRs (SNR $\geq$ 15), we can see that the FTA method is very effective at estimating the timing-offset, and that the performance of our proposed method is very close to the FTA method. However, under low SNRs(SNR$<$10), our proposed method has much better performance than the FTA method due to the poor anti-noise capability of the FTA method.

E. PERFORMANCE OF CFO ESTIMATION

The performance of the CFO estimator can be evaluated using the normalized residual CFO, which is given by

$$E_n = E\{|\Delta\hat{f} - \Delta f|\}/f_\Delta \tag{23}$$

where $\Delta\hat{f}$ is the estimated CFO, Δf is the real CFO and f_Δ is the sub-carrier spacing.

The performance comparison between CFO estimators is shown in Figure 14 and Figure 15. The performance of the proposed CFO estimator in the case that the $N/2$-point

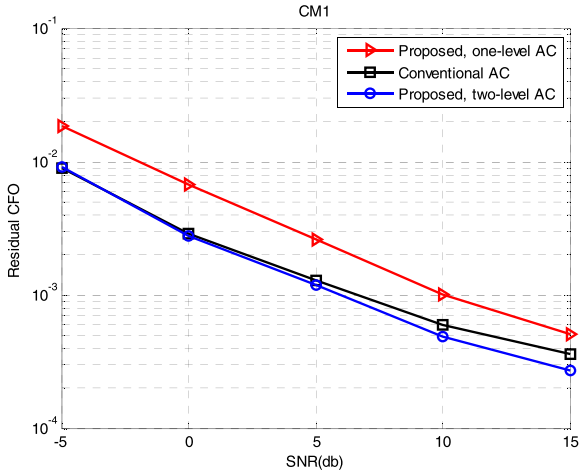

FIGURE 14. Comparison of residual CFOs between timing offset estimation methods, in the UWB CM1 channel.

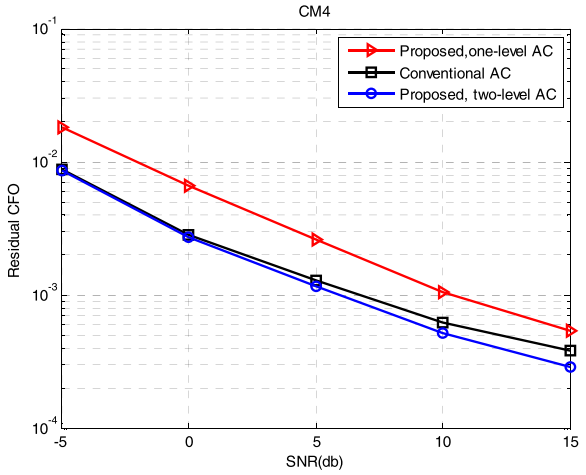

FIGURE 15. Comparison of residual CFOs between timing offset estimation methods, in the UWB CM4 channel.

AC with one-level serial structure and the case that the $N/2$-point AC with two-level serial structure are simulated, respectively. The performance of a conventional N-point AC based CFO estimator is also included in the comparison. The simulation is done in UWB channels CM1 and CM4, by assuming the normalized initial CFO is 0.035. As the CFO achieved from the two-level serial structure based $N/2$-point AC has higher accuracy than the conventional AC, the proposed CFO estimator based on the two-level serial structure based $N/2$-point AC has even a slightly better performance than the conventional estimator in SNR>5db environments (shown in Figure 14 and Figure 15). More importantly, the $N/2$-point AC operation can be implemented with much lower complexity.

IV. CONCLUSIONS

In this paper, we presented a synchronization design for the MB-OFDM UWB based vehicular communication. This design aims to provide a comprehensive synchronizer with low complexity and high performance. By analyzing the characteristics of the individual functions, an overall architecture based on two common blocks has been proposed, which divides the sub-functions into amplitude-detection-based functions and phase-detection-based functions. All the amplitude-detection-based functions were implemented based on a simplified CC based MF structure, and a serial structure based AC block was designed exclusively for CFO estimation, which gives greater flexibility to the CFO estimation design. Based on the MF, a TFC identification structure with low complexity, and an effective joint structure of packet detection and timing offset estimation have been proposed. A CFO estimation structure with low complexity has also been proposed. Evaluation results have shown that the proposed synchronizer has high performance with low complexity.

APPENDIX A

Assuming that preamble pattern i is currently loaded in the MF and $q_r(k)(k = 1, \ldots, 128)$ are the signs of the samples of the received symbol, two scenarios of the outputs of the MF should be considered:

1) The PS symbol of preamble pattern i is received. In this case, most $q_r(k)q_c(k) = -1$ occur on the coefficients with small $w_c(k)(w_c(k) < 1)$, and most $q_r(k)q_c(k) = 1$ occur on the coefficients with large $w_c(k)$. Therefore, $q_r(k)q_c(k)w_c(k)$ can be approximately simplified as

$$q_r(k)q_c(k)w_c(k) = \begin{cases} -1/2 & q_r(k)q_c(k) = -1 \\ 3/2 & q_r(k)q_c(k) = 1 \end{cases} \quad (24)$$

In this case, let $P_1(\lambda) = P[G_i(n) > \lambda]$. The mean of $P[q_r(k)q_c(k) = 1]$ is approximately $1/2erfc(-\bar{m}/\sqrt{2\sigma^2})$ [33], where $\bar{m}$ is the mean of $|c(k)|$ $(k = 1, \ldots, 128)$. According to the central limit theorem, $P_1(\lambda)$ is given by

$$P_1(\lambda) = 1-\Phi\left[\frac{\frac{N+2\lambda}{4} - \frac{1}{2}erfc\left(\frac{-\bar{m}}{\sqrt{2\sigma^2}}\right)N}{\sqrt{\frac{1}{2}erfc\left(\frac{-\bar{m}}{\sqrt{2\sigma^2}}\right)\left[1-\frac{1}{2}erfc\left(\frac{-\bar{m}}{\sqrt{2\sigma^2}}\right)\right]N}}\right] \quad (25)$$

where $\Phi(x) = \int_{-\infty}^{x} \frac{1}{\sqrt{2\pi}} e^{-\frac{1}{2}t^2} dt$.

2) The PS symbol of preamble pattern $j(j \neq i)$ is received, or noise is received. In this case, let $P_2(\lambda) = P[G_i(n) > \lambda]$. The samples of the received symbol are uncorrelated with the coefficients of preamble pattern i. By quantizing $q_r(k)q_c(k)w_c(k)$ as 1 or -1, $P_2(\lambda)$ can be given by

$$P_2(\lambda) = 1 - \Phi\left(\frac{\frac{N+\lambda}{2} - \frac{1}{2}N}{\frac{1}{2}\sqrt{N}}\right) \quad (26)$$

APPENDIX B

In Figure 6, $D(i)$ can be seen as the results of a modified MF, which uses the coefficients of multiple repeated PS symbols to correlate with multiple received symbols.

Therefore, according to (25) in appendix A, if PS symbols are present, $P[D(i) > \lambda]$ can be given by

$$P_3(i,\lambda) = 1-\Phi\left[\frac{\frac{iN+2\lambda}{4} - \frac{1}{2}erfc\left(\frac{-\bar{m}}{\sqrt{2\sigma^2}}\right)iN}{\sqrt{\frac{1}{2}erfc\left(\frac{-\bar{m}}{\sqrt{2\sigma^2}}\right)\left[1-\frac{1}{2}erfc\left(\frac{-\bar{m}}{\sqrt{2\sigma^2}}\right)\right]iN}}\right] \tag{27}$$

According to (26) in appendix A, if noise is received, $P[D(i) > \lambda]$ can be given by

$$P_4(i,\lambda) = 1-\Phi\left(\frac{\frac{iN+\lambda}{2} - \frac{1}{2}iN}{\frac{1}{2}\sqrt{iN}}\right) \tag{28}$$

REFERENCES

[1] J. Wan, J. liu, Z. Shao, A. V. Vasilakos, M. Imran, and K. Zhou, "Mobile crowd sensing for traffic prediction in Internet of vehicles," *Sensors*, vol. 16, no. 1, p. 88, Jan. 2016.

[2] C. Huang, C. Yang, and Y. Lin, "An adaptive video streaming system over a cooperative fleet of vehicles using the mobile bandwidth aggregation approach," *IEEE Syst. J.*, vol. 10, no. 2, pp. 568–579, Jun. 2014.

[3] X. Ge, H. Cheng, G. Mao, Y. Yang, and S. Tu, "Vehicular communications for 5G cooperative small cell networks," *IEEE Trans. Veh. Technol.*, vol. 65, no. 10, pp. 7882–7894, Oct. 2016.

[4] A. E. Gueraa, A. Darif, R. Saadane, and D. Aboutajdine, "An efficient transceiver for vehicular ad hoc network based on IR-UWB," in *Proc. WCCS*, Nov. 2014, pp. 220–224.

[5] T. G. Krebesz, G. Kolumban, C. K. Tse, F. Lau, and H. Dong, "Use of UWB impulse radio technology in in-car communications: Power limits and optimization," *IEEE Trans. Veh. Technol.*, to be published, doi: 10.1109/TVT.2017.2647849.

[6] *Multiband OFDM Physical Layer Specification*, WiMedia Alliance, San Ramon, CA, USA, Mar. 2004.

[7] *High Rate Ultra Wideband PHY and MAC Standard*, Standard ECMA-368 Dec. 2008.

[8] A. Batra, J. Balakrishnan, G. R. Aiello, J. R. Foerster, and A. Dabak, "Design of a multiband OFDM system for realistic UWB channel environments," *IEEE Trans. Microw. Theory Techn.*, vol. 52, no. 9, pp. 2123–2138, Sep. 2004.

[9] X. Ge, S. Tu, T. Han, and Q. Li, "Energy efficiency of small cell backhaul networks based on Gauss–Markov mobile models," *IET Netw.*, vol. 4, no. 2, pp. 158–167, 2015.

[10] H. Steendam and M. Moeneclaey, "Synchronization sensitivity of multicarrier systems," *Eur. Trans. Commun.*, vol. 15, no. 3, pp. 223–234, May 2004.

[11] X. Zhang, J. Liu, H. Li, and B. Himed, "Maximum likelihood synchronization for DVB-T2 in unknown fading channels," *IEEE Trans. Broadcast.*, vol. 61, no. 4, pp. 615–624, Dec. 2015.

[12] W. Fan, C. Choy, and K. Leung, "Robust and low complexity packet detector design for MB-OFDM UWB system," in *Proc. ISCAS*, Taipei, China, May 2009, pp. 693–696.

[13] Q. Jing, M. Cheng, Y. Lu, W. Zhong, and H. Yao, "Pseudo-noise preamble based joint frame and frequency synchronization algorithm in OFDM communication systems," *J. Syst. Eng. Electron.*, vol. 25, no. 1, pp. 1–9, Feb. 2014.

[14] B. Awoseyila, C. Kasparis, and B. G. Evans, "Robust time-domain timing and frequency synchronization for OFDM systems," *IEEE Trans. Consum. Electron.*, vol. 55, no. 2, pp. 391–399, Aug. 2009.

[15] M. Karim, M. Othman, and E. Zahedi, "Packet synchronization structure with peak detection algorithm for MB-OFDM UWB," in *Proc. IEEE ICSE*, Kuala Lumpur, Malaysia, Oct. 2006, pp. 388–391.

[16] C. W. Yak, Z. Lei, S. Chattong, and T. T. Tjhung, "Timing synchronization for ultra-wideband (UWB) multi-band OFDM systems," in *Proc. VTC Fall*, Dallas, TX, USA, Sep. 2005, pp. 1599–1603.

[17] J. Lai, A. Wu, and W. Chen, "A systematic design approach to the band-tracking packet detector in OFDM-based ultra wideband systems," *IEEE Trans. Veh. Technol.*, vol. 56, no. 6, pp. 3791–3806, Nov. 2009.

[18] A. Mohebbi, H. Abdzadeh-Ziabari, and M. G. Shayesteh, "Novel coarse timing synchronization methods in OFDM systems using fourth-order statistics," *IEEE Trans. Veh. Technol.*, vol. 64, no. 5, pp. 1904–1917, Jul. 2014.

[19] Y. Liu, H. Yu, F. Ji, F. Chen, and W. Pan, "Robust timing estimation method for OFDM Systems with reduced complexity," *IEEE Commun. Lett.*, vol. 18, no. 11, pp. 1959–1962, Nov. 2014.

[20] W. Fan and C.-S. Choy, "Robust, low-complexity, and energy efficient downlink baseband receiver design for MB-OFDM UWB system," *IEEE Trans. Circuits Syst. I, Reg. Papers*, vol. 59, no. 2, pp. 399–408, Feb. 2012.

[21] Z. Ye, C. Duan, P. V. Orlik, J. Zhang, and A. A. Abouzeid, "A synchronization design for UWB-based wireless multimedia systems," *IEEE Trans. Broadcast.*, vol. 56, no. 2, pp. 211–225, Mar. 2010.

[22] Y. Li, H. Minn, and T. Jacobs, "Frequency offset estimation for MB-OFDM-based UWB systems," *IEEE Trans. Commun.*, vol. 56, no. 6, pp. 968–979, Jun. 2008.

[23] S. Lv, Z. Qian, Y. Dong, and Q. Li, "A timing synchronization scheme for MB-OFDM based UWB systems," in *Proc. ICNISC*, Wuhan, China, Jan. 2015, pp. 536–539.

[24] Y. Yao, X. Dong, and N. Tin, "Design and analysis of timing synchronization in block transmission UWB systems," *IEEE Trans. Commun.*, vol. 59, no. 6, pp. 1686–1696, Jun. 2011.

[25] M. M. U. Gul, X. Ma, and S. Lee, "Timing and frequency synchronization for OFDM downlink transmissions using Zadoff–Chu sequences," *IEEE Trans. Wireless Commun.*, vol. 14, no. 3, pp. 1716–1729, Mar. 2015.

[26] T. M. Schmidl and D. C. Cox, "Robust frequency and timing synchronization for OFDM," *IEEE Trans. Commun.*, vol. 45, no. 12, pp. 1613–1621, Dec. 1997.

[27] H. Minn, V. K. Bhargava, and K. B. Letaief, "A robust timing and frequency synchronization for OFDM systems," *IEEE Trans. Wireless. Commun.*, vol. 2, no. 4, pp. 822–839, Jul. 2003.

[28] J. Liu, J. Wan, Q. Wang, P. Deng, K. Zhou, and Y. Qiao, "A survey on position-based routing for vehicular ad hoc networks," *Telecommun. Syst.*, vol. 62, no. 1, pp. 15–30, 2016.

[29] J. Liu, J. Wan, Q. Wang, D. Li, Y. Qiao, and H. Cai, "A novel energy-saving one-sided synchronous two-way ranging algorithm for vehicular positioning," *Mobile Netw. Appl.*, vol. 20, no. 5, pp. 661–672, Oct. 2015.

[30] "Revision of part15 of the commission's rules regarding ultra-wideband transmission system," FCC, Washington, DC, USA, Tech. Rep. FCC s02-48, Jul. 2002.

[31] J. Balakrishnan, A. Batra, and A. Dabak, "A multi-band OFDM system for UWB communication," in *Proc. UWBST*, Reston, VA, USA, Nov. 2003, pp. 354–358.

[32] *Channel Modeling Sub-Committee Report Final*, IEEE Standard P802.15-SG3a-02/490r1, Feb. 2003.

[33] X.-W. Yin and H.-Z. Tan, "A power-efficient synchronization scheme for the MB-OFDM-based UWB systems," *EUR. J. Wireless Commun. Netw.*, vol. 2015, no. 1, p. 14, Jan. 2015.

[34] R. Bose, "Ultra wideband indoor channel modeling for personal area networking," in *Proc. EuCAP* Nice, France, Nov. 2006, pp. 1–4.

[35] D. Sen, S. Chakrabarti, and R. V. Raja Kumar, "Symbol timing synchronization for ultra-wideband (UWB) multi-band OFDM (MB-OFDM) systems," in *Proc. COMSWARE*, Bangalore, India, Jan. 2008, pp. 200–203.

[36] A. Batra *et al.*, "Multiband OFDM physical layer proposal for IEEE 802.15 task group 3a," WiMedia Alliance, San Ramon, CA, USA, Tech. Rep., Mar. 2004.

XIUWEN YIN received the B.S. degree in computer science and technology from Nanchang University, Nanchang, China, in 2005, the M.S. degree in computer software and theory from the Guangdong University of Technology, Guangzhou, China, in 2010, and the Ph.D. degree in communication and information system from Sun Yat-sen University, Guangzhou, in 2015. He is currently a Lecturer with the School of Automation, Guangdong University of Technology. His current research interests include integrated circuit design, digital signal processing, and broadband wireless communication.

JIANQI LIU (M'11) received the B.S. degree in computer science and technology from Nanchang University, Nanchang, China, and the M.S. degree in computer software and theory and the Ph.D. degree in control science and engineering from the Guangdong University of Technology, Guangzhou, China. He is currently an Associate Professor with the School of Information Engineering, Guangdong Mechanical & Electrical College, China. His current research interests include the Internet of Vehicle, wireless sensor networks, Internet of Things, and cyber-physical systems.

YONGFENG SU received the B.S. degree in computer science and technology from Nanchang University, Nanchang, China, and the M.S. degree in computer software and theory from the Guangdong University of Technology, Guangzhou, China. His current research interests include the Internet of Vehicle, wireless sensor networks, and broadband wireless communication.

XIAOMING XIONG received the B.S. degree in electrical engineering from the South China University of Technology, Guangzhou, China, in 1982, and the Ph.D degree in electrical engineering and computer science from the University of California at Berkeley, Berkeley, CA, USA, in 1988. He is currently a Professor with the School of Automation, Guangdong University of Technology, Guangzhou. His current research interests include integrated circuit and system-on-chip design, computer aided design and electronic design automation, computer algorithms, graph theory, and computational geometry.

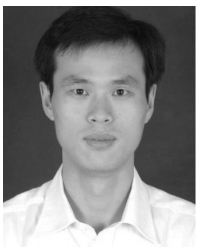

GUOHUA XIONG received the B.S. degree in computer science and technology from Nanchang University, Nanchang, China, in 2005, and the M.S. degree in computer software and theory from the Guangdong University of Technology, Guangzhou, China, in 2008. He is currently a Lecturer with the Guangdong Construction Polytechnic, Guangzhou. His current research interests include software engineering and software automation, data mining, and cloud computing.